Excited-state dynamics and energy transfers in (Ca,Zr)-substituted $Gd_3Ga_5O_{12}$ single crystals doped with Cr^{3+} and Tm^{3+} ions

1991 J. Phys.: Condens. Matter 3 203

(http://iopscience.iop.org/0953-8984/3/2/007)

J. Phys.: Condens. Matter 3 (1991) 203–214. Printed in the UK

Excited-state dynamics and energy transfers in (Ca, Zr)-substituted $Gd_3Ga_5O_{12}$ single crystals doped with Cr^{3+} and Tm^{3+} ions

A Brenier, C Madej, C Pedrini and G Boulon
Laboratoire de Physico-Chimie des Matériaux Luminescents, URA CNRS 442, Université Lyon I, 43 Bd du 11 Novembre 1918, 69622 Villeurbanne, France

Received 19 July 1990, in final form 3 October 1990

Abstact. The excited-state dynamics of Cr^{3+} and Tm^{3+} ions in (Ca, Zr)-substituted $Gd_3Ga_5O_{12}$ garnets and the energy transfer mechanisms between these impurity ions were studied at room temperature under various laser excitations. The single crystals have been grown in our laboratory by using the Czochralski method under nitrogen and oxygen flow. The $Cr^{3+} \rightarrow Tm^{3+}$ energy transfers and the $Tm^{3+} \rightarrow Tm^{3+}$ cross-relaxation processes were analysed in detail and their efficiencies calculated as a function of the Tm^{3+} concentrations.

1. Introduction

It is well known that eye-safe 2 μm infrared solid-state lasers are usually obtained from the $^5I_7 \rightarrow {}^5I_8$ transition of Ho^{3+} impurity ions in various fluorides and garnets. Most often, the fluorescence of the Ho^{3+} ions is sensitized by erbium and thulium ions in fluorides and also by chromium ions in garnets. Many continuous-wave (CW) and Q-switched laser operations have been proved in several holmium-doped crystals at cryogenic as well as room temperature [1–6] and recently more especially with laser diode pumping [7]. It was shown recently that laser radiation around 2 μm can also be obtained from the $^3F_4 \rightarrow {}^3H_6$ transition of Tm^{3+} in garnets [8, 9].

Therefore garnets doped with chromium, thulium and holmium ions are very interesting laser materials for generating eye-safe 2 μm laser transitions under cross-pumping either in the visible region via Cr^{3+} or in the 800 nm near-infrared region by diode laser arrays via Tm^{3+}. In the first case of pumping, the slope efficiencies can be increased if the rate of the $Cr^{3+} \rightarrow Tm^{3+}$ energy transfer is improved. The latter depends on the overlap between the emission of chromium ions and the $^3H_4$ absorption of thulium. In $Y_3Al_5O_{12}$ (YAG), where the crystal field is strong, the transfer of energy takes place from the ^2E electronic state of the chromium ions and the transfer rate is small. In gallium garnets, the chromium ions are imbedded in an intermediate crystal field so that the $Cr^{3+} \rightarrow Tm^{3+}$ energy transfer is much more efficient since it originates from the $^4T_2$ level of Cr^{3+}. The best systems are scandium-based gallium garnets like $Y_3Sc_2Ga_3O_{12}$ (YSGG) and $Gd_3Sc_2Ga_3O_{12}$ (GSGG) since Sc^{3+} is a large ion giving rise to larger lattice constants and therefore weaker crystal fields. However, scandium being very expensive, such systems can hardly be considered as commercial laser crystals.

0953-8984/91/020203 +12 $03.50

Alternatives to scandium-based garnets are garnet crystals in which the crystal field is lowered by the insertion of some large ions at the Gd and octahedral Ga sites in $Gd_3Ga_5O_{12}$ (GGG). We have grown crystals of so-called (Ca, Zr)-substituted GGG [10] in which Ca^{2+} and Zr^{4+} ions are introduced to increase the lattice parameter. This paper is dedicated to a detailed study of the excited-state dynamics of Cr^{3+} and Tm^{3+} ions and of the $Cr^{3+} \rightarrow Tm^{3+}$ energy transfers in such single crystals. The present study is a first necessary step in the final optical investigation of the chromium, thulium and holmium triply doped systems, which will be presented in a forthcoming paper.

2. Crystal growth

Mateika *et al* [10] have succeeded in producing (Ca, Zr)-substituted GGG (CZ-GGG) of the formula $(Gd_{3-x}Ca_x)(Ga_{2-y-z}Zr_yGd_z)Ga_3O_{12}$, and only one composition with $x = y = 0.45$ and $z = 0$ was found to melt congruently. Allibert *et al* [11] had previously studied the Gd_2O_3–Ga_2O_3 system, and the congruently melting composition was actually found to be equal to $Gd_{3.05}Ga_{4.95}O_{12}$. Finally, we have grown crystals of the composition $(Gd_{2.55}Ca_{0.45})(Ga_{1.5}Zr_{0.45}Gd_{0.05})Ga_3O_{12}$.

The crystals have been grown by the Czochralski technique under a gas flow of nitrogen ($480\,l\,h^{-1}$) and oxygen ($4.8\,l\,h^{-1}$) in order to suppress gallium oxide decomposition and iridium losses from the crucible [12, 13]. The pull rate was 0.4 cm h^{-1} and the rotation rate varied according to the crystal length from 6 to 15 rpm. The typical crystal size was 3 cm diameter and 10 cm length. The crystals were pulled along the ⟨1 1 1⟩ axis.

The doping with Tm^{3+} and Cr^{3+} ions has been done by adding Tm_2O_3 and Cr_2O_3 to the melt. We have replaced Gd by $Gd_{1-x}Tm_x$ (with $x = 0, 0.005, 0.01, 0.03, 0.07$). We have introduced 0.0225 mol of Cr^{3+} ions (in octahedral sites) per mol of crystal so that the amount of Cr^{3+} represents 0.5% of Ga^{3+} ions (including both octahedral and tetrahedral sites). Finally, knowing the segregation coefficient of Cr^{3+} in such crystals (2.8) [14], the starting composition of the baths was

$2.6(1 - x)$ mol of Gd^{3+}

$2.6x$ mol of Tm^{3+}

0.45 mol of Ca^{2+} and Zr^{4+}

$4.5(1 - 0.005)$ mol of Ga^{3+}

$4.5(0.005)/2.8$ mol of Cr^{3+}

leading to 1 mol of crystal of composition

$$(TR_{2.55}Ca_{0.45})(Ga_{1.4775}Cr_{0.0225}Zr_{0.45}TR_{0.05})Ga_3O_{12}$$

with $TR = Gd_{1-x}Tm_x$.

The impurity ion concentration $C(x)$ along the axis of the crystal and the segregation coefficient k are related according to the well known expression

$$C(x)/C_0 = [1 - g(x)]^{k-1} \tag{1}$$

where $C_0 = C(0)$ at the beginning of the crystal and g is the crystallized mass fraction. Exponent k can be directly calculated from (1) since C/C_0 is experimentally deduced from absorption measurements for Cr^{3+} and Tm^{3+} ions or from x-ray fluorescence

Table 1. Segregation coefficients k for various impurity ions in (Ca, Zr)-substituted GGG.

Ion	Cr^{3+}	Tm^{3+}	Ca^{2+}	Zr^{4+}
k	2.8	1.1	0.95	0.95

Table 2. Cr^{3+} and Tm^{3+} concentrations of the various samples used in the optical study.

	C (10^{20} cm^{-3})	
x (%)	Cr^{3+}	Tm^{3+}
0	0.5	0
0.5	0.7	0.6
1	0.8	1.2
3	0.7	3.4
7	0.8	9.3

analysis for Ca^{2+} and Zr^{4+} ions. The k values for each impurity ion are given in table 1. It is fortunate to find the expected k value for Cr^{3+}. For the other ions, k is nearly 1, justifying *a posteriori* the nominal concentrations chosen in the starting composition of the baths.

Then $C(x)$ can be easily deduced from (1) since C_0 is calculated from

$$k = C(0)/C'(0) \tag{2}$$

where $C'(0)$ is the impurity ion concentration of the bath at the beginning of crystal growth. The Cr^{3+} and Tm^{3+} concentrations of the samples used in the optical study are gathered in table 2. For all the co-doped systems, the Cr^{3+} concentration was kept nearly constant ($(0.7–0.8) \times 10^{20}$ cm^{-3}) whereas the Tm^{3+} concentration varies strongly from 0.6×10^{20} to 9.3×10^{20} cm^{-3}.

3. Experimental optical techniques

Emission spectra of chromium and thulium ions were recorded by exciting with a 1 kW halogen lamp followed by an interference filter or a Jobin-Yvon H20 monochromator for selective excitation. The fluorescence was analysed with a Jobin-Yvon H20 IR or H20 FIR monochromator, depending on the spectral range to be investigated, and detected by an OptoElectronics cooled lead sulphide detector OTC-22S-8. The signal was chopped and fed into an EGG 128 A lock-in amplifier and recorded with a plotter.

The absorption data were measured using a Cary UV–visible–NIR spectrophotometer, model 2300, covering the wavelength range from 185 to 3152 nm.

Fluorescence lifetime measurements used as optical excitation source a Q-switched Nd^{3+} : YAG pumped-dye laser (Datachrom model from Quantel) associated with a hydrogen Raman cell to produce infrared radiation up to 2 μm. The fluorescence was detected

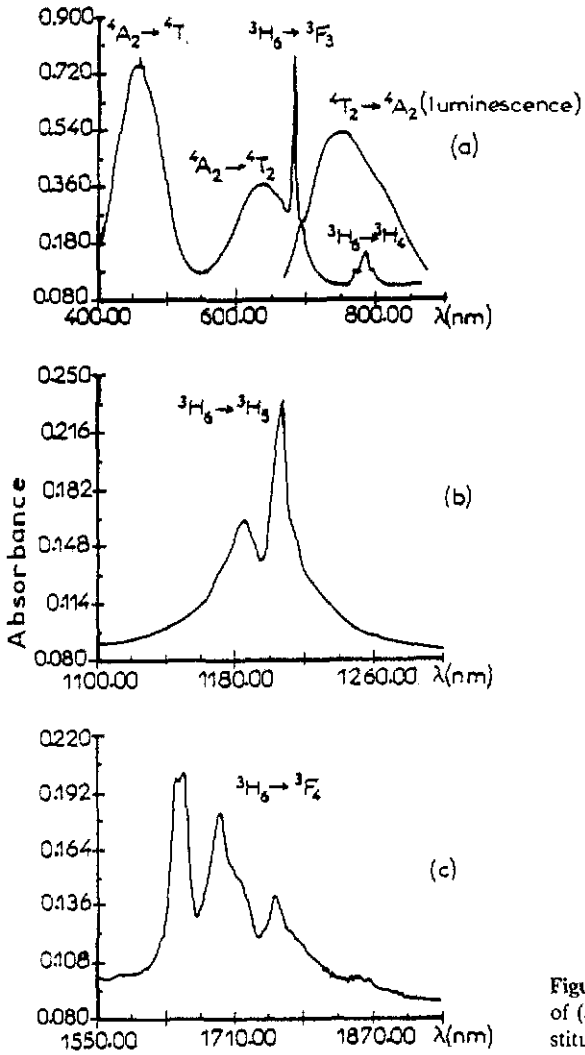

Figure 1. Absorption spectra at room temperature of (*a*) Cr^{3+} and (*a*, *b*, *c*) Tm^{3+} in (Ca, Zr)-substituted $Gd_3Ga_5O_{12}$ crystals.

through interference filters by a fast-response (0.5 μs) Judson Infrared Inc. model J10-D InSb photodiode cooled to liquid-nitrogen temperature and the lifetime data were recorded with a Le Croy 9400 Dual 125 MHz digital oscilloscope.

4. Excited-state dynamics

4.1. Spectral analysis and energy levels

The absorption spectra at room temperature are reported in figure 1. In the 400–900 nm wavelength range (figure 1(*a*)), the two broad bands are assigned to the $^4A_2 \rightarrow {}^4T_1$ and $^4A_2 \rightarrow {}^4T_2$ transitions of Cr^{3+} in the green and red regions, respectively. Narrow lines are superimposed due to Tm^{3+} ions, the stronger ones being attributed to the $^3H_6 \rightarrow {}^3F_2$,

$^3F_3$ transitions in the red and to the $^3H_6 \rightarrow {}^3H_4$ transition in the near-infrared. In the same graph is represented the emission band of Cr^{3+} corresponding to the $^4T_2 \rightarrow {}^4A_2$ transition. It is clear that the important overlap between this Cr^{3+} emission band and the $^3H_6 \rightarrow {}^3H_4$ absorption lines of Tm^{3+} is very propitious to efficient $^4T_2(Cr^{3+}) \rightarrow {}^3H_4$ (Tm^{3+}) energy transfer. Other absorption lines of Tm^{3+} ions are also observed in the infrared region around 1200 nm (figure 1(*b*)) and 1700 nm (figure 1(*c*)) and assigned to $^3H_6 \rightarrow {}^3H_5$ and $^3H_6 \rightarrow {}^3F_4$ transitions, respectively.

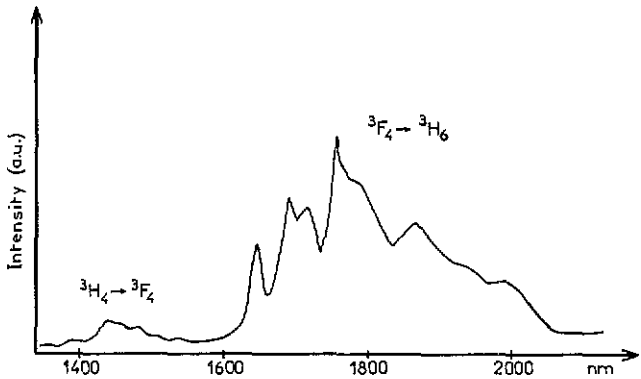

Figure 2. Infrared fluorescence spectrum of Tm^{3+} ions in (Ca, Zr)-substituted $Gd_3Ga_5O_{12}$ at room temperature under broad-band excitation in the visible region.

The infrared fluorescence spectrum of Tm^{3+} ions is represented in figure 2. The two groups of emission lines are due to the $^3H_4 \rightarrow {}^3F_4$ and $^3F_4 \rightarrow {}^3H_6$ transitions as indicated in the figure. As expected, the $^3H_5 \rightarrow {}^3H_6$ emission is not observed because of the very effective non-radiative $^3H_5 \rightarrow {}^3F_4$ transition. These fluorescences will be involved in the study of the lowest excited-state dynamics of Tm^{3+} ions.

These absorption and emission spectra were used to deduce the energy level scheme represented in figure 3.

4.2. Dynamics of Tm^{3+} ions under direct excitation

4.2.1. $^3F_4$ and $^3H_5$ excited states. After direct excitation of Tm^{3+} ions in the $^3F_4$ or $^3H_5$ levels, the fluorescence of the $^3F_4 \rightarrow {}^3H_6$ transition decays exponentially without risetime just after the laser excitation pulse. The time constant τ_3 of the decay is about constant and equal to 11.25 ms for Tm^{3+} concentrations varying from 0.5 to 3%. This means that, for these low concentrations, the energy diffusion is weak or does not induce energy loss. At a higher Tm^{3+} concentration (7%), τ_3 falls to 6 ms, indicating that the energy migration is now really effective. The absence of fluorescence risetime under $^3H_5$ excitation allows us to estimate a short $^3H_5$ lifetime (less than 1 μs) due to a rapid $^3H_5 \rightarrow {}^3F_4$ multiphonon relaxation ($^3H_5 - {}^3F_4$ energy gap $\simeq 2200\ cm^{-1}$).

4.2.2. $^3H_4$, $^3H_6 \rightarrow {}^3F_4$, $^3F_4$ cross-relaxation mechanism. The time dependence of the $^3H_4$ population when this level is directly excited has been studied by considering the fluorescence of the $^3H_4 \rightarrow {}^3F_4$ transition (figure 2), which can be well separated by interference filters from the excitation wavelength. We do not observe risetimes and

the decays are non-exponential and shorten strongly when the Tm^{3+} concentration increases. These results are interpreted by the $^3H_4$, $^3H_6 \rightarrow {}^3F_4$, $^3F_4$ cross-relaxation mechanism represented in figure 3, and which is usually involved and has been proved to occur in many Tm^{3+}-doped crystals [5, 8, 15, 16]. In the present case, this transfer is phonon-assisted since the gaps $^3H_4$–$^3F_4 = 6600\ cm^{-1}$ and $^3F_4$–$^3H_6 = 6000\ cm^{-1}$ are slightly different.

Because of the non-exponential character of the decays whatever the Tm^{3+} concentration considered (0.5, 1, 3, 7%), we are not dealing with a very fast energy diffusion among Tm^{3+} ions. Therefore all Tm^{3+} sites are not equivalent and Grant's procedure [17] leading to the description of energy transfers by rate equations cannot be applied. Considering that each Tm^{3+} ion in the $^3H_4$ excited state is surrounded by a uniform statistical distribution of Tm^{3+} ions in the ground state $^3H_6$, with which it is in dipole–dipole interaction, and supposing a diffusion-limited transfer regime, we have used the Yokota and Tanimoto expression [18] to describe our experimental data:

$$N_2(t) = N_2(0) \exp\left[-\frac{t}{\tau_2} bt^{1/2} \left(\frac{1 + 10.87x + 15.50x^2}{1 + 8.743x}\right)^{3/4}\right] \tag{3}$$

with

$$b = \tfrac{4}{3}\pi^{3/2} C R_0^3 / \tau_2^{1/2}. \tag{4}$$

Here τ_2' is the lifetime of the $^3H_4$ level (in the absence of transfer), C is the concentration of Tm^{3+} in the ground state (see table 2) and R_0 is the radius of the 'sphere of influence'

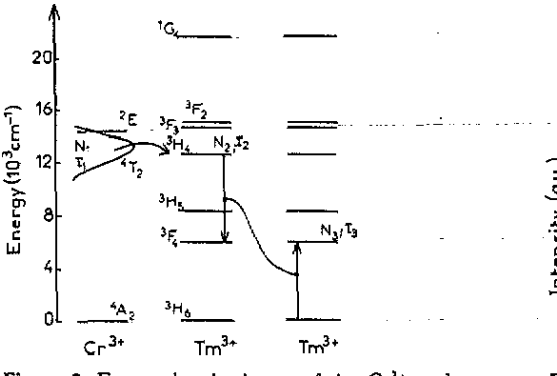

Figure 3. Energy level scheme of the Cr^{3+} and Tm^{3+} ions and main energy transfers.

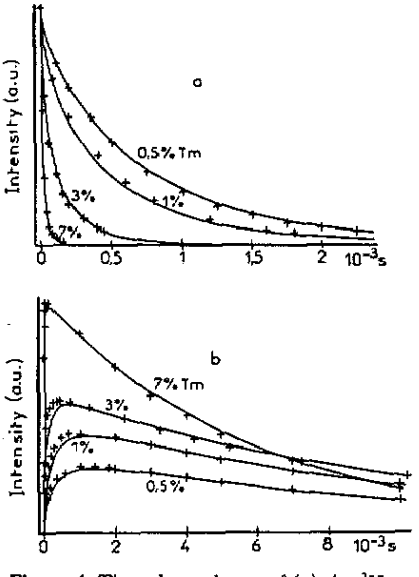

Figure 4. Time dependence of (*a*) the $^3H_4 \rightarrow {}^3F_4$ fluorescence and (*b*) the $^3F_4 \rightarrow {}^3H_6$ fluorescence in (Ca, Zr)-substituted $Gd_3Ga_5O_{12}$ at room temperature for various Tm^{3+} concentrations. Full curves represent the best fits to experimental data (+).

defined as the distance at which the energy transfer rate $W_{DA}(R)$ is equal to the decay rate τ_2 of the donor:

$$W_{DA}(R) = C_{DA}^{(6)}/R_{DA}^6 = (1/\tau_2)(R_0/R_{DA})^6. \tag{5}$$

R_0 can be calculated if the dipole–dipole term $C^{(6)}$ is known, from

$$R_0^6 = C_{DA}^{(6)} x \tau_2 \tag{6}$$

$$x = D(C_{DA}^{(6)})^{-1/3} t^{2/3} = D R_0^{-2} \tau_2^{1/3} t^{2/3} \tag{7}$$

where D is the diffusion coefficient.

The long-time behaviour of equation (3) is referred to as diffusion-limited relaxation, and is characterized by exponential decay at long times. The fluorescence decay function becomes

$$N_2(t) = N_2(0) \exp(-1/\tau_2 - 1/\tau_D) \tag{8}$$

with

$$1/\tau_D \simeq 4\pi C (C_{DA}^{(6)})^{1/4} D^{3/4}. \tag{9}$$

The diffusion coefficient is related to the rate of energy transfer from D ion to nearest neighbour D ion [19]:

$$D = W_{DD} R_{min}^2. \tag{10}$$

Then

$$D \propto (C_{DD}/R^6)\, R^2 = C_{DD}/R^4 \propto C^{4/3} \tag{11}$$

since $C \propto R^{-3}$.

Finally the diffusion coefficient D is found to be proportional to $C^{4/3}$ and we can write:

$$D = kC^{4/3}. \tag{12}$$

The best fit to experimental data (figure 4(*a*)) has been obtained with the three free parameters of the model: $\tau_2 = (1.065 \pm 0.01) \times 10^{-3}$ s, $R_0 = 10.5 \pm 0.1$ Å and $k = (1.55 \pm 0.01) \times 10^{-39}$ cm^6 s^{-1}.

The quantum efficiency η_{CR} of the cross-relaxation process is given by

$$\eta_{CR} = 1 - \frac{1}{N_2(0)\tau_2} \int_0^\infty N_2(t)\, dt. \tag{13}$$

The values of η_{CR} calculated from equation (13) are gathered in table 3. One can see that the cross-relaxation becomes the dominant process when the Tm^{3+} concentration exceeds 1% and completely governs the excited-state dynamics at higher concentrations above 7%.

Table 3. Quantum efficiencies of the $Tm^{3+} \rightarrow Tm^{3+}$ cross-relaxation η_{CR} and $Cr^{3+} \rightarrow Tm^{3+}$ energy transfer η_T processes (±1%).

x (%)	0.5	1	3	7
η_{CR} (%)	36	59	89	98
η_T (%)	27	45	77	94

The excitation of Tm^{3+} ions in the $^3H_4$ excited state also leads to the fluorescence emission of the $^3F_4$ level corresponding to the $^3F_4 \rightarrow {}^3H_6$ transition (figure 2). The fluorescence decay, illustrated in figure 4(*b*), is preceded by a rise, the time constant of which shortens strongly when the Tm^{3+} concentration increases. The time dependence of the $^3F_4$ population $N_3(t)$ may be written as

$$\dot{N}_3(t) = -N_3/\tau_3 + AN_2 - (2N_2/\tau_2 + \dot{N}_2) \tag{14}$$

with the initial condition $N_3(0) = 0$, where $N_2(t)$ is given by equation (3) and τ_3 is experimentally known (11.25 ms). The first term represents the relaxation of the $^3F_4$ level and the second one describes the feeding of $^3F_4$ by the $^3H_4$ de-excitation directly or via the $^3H_5$ level (A stands for the $^3H_4$ de-excitation probability). The third term is a way to represent the contribution of the cross-relaxation process to the time dependence of N_3. In the identity equation

$$\dot{N}_2 \equiv -N_2/\tau_2 + (N_2/\tau_2 + \dot{N}_2) \tag{15}$$

the second term actually describes the cross-relaxation. The factor 2 in equation (14) takes into account the fact that one $^3H_4$ Tm^{3+} excited ion leads to two $^3F_4$ Tm^{3+} excited ions. Obviously, the second and third terms both contribute to the rise of the fluorescence. We have solved the differential equation (14) by neglecting the second term. For high Tm^{3+} concentrations (3 and 7%), it is clear that the cross-relaxation process is predominant (table 3) and this approximation is justified. For lower Tm^{3+} concentrations, it should be noted that the fluorescence decays of the $^3H_4$ level appear to be more exponential. This means that N_2 and $\dot{N}_2$ are nearly proportional and that the second and third terms of equation (14) are also themselves proportional.

The solution of equation (14), in which $A = 0$, is the following:

$$N_3(t) = 2N_2(0)\exp(-t/\tau_3) - 2N_2(t) + 2\left(\frac{1}{\tau_3} - \frac{1}{\tau_2}\right)\int_0^t N_2(t')\exp\left(\frac{t'-t}{\tau_3}\right)\mathrm{d}t'. \tag{16}$$

$N_2(t)$ is of course calculated from (3) and the integral is solved numerically. One can see in figure 4(*b*) that the experimental data are rather well described by (16). It can be noted that no new fitting parameters had to be used for this description.

4.3. $Cr^{3+} \rightarrow Tm^{3+}$ energy transfers

The Cr^{3+} ions have been excited at 640 nm in the $^4A_2 \rightarrow {}^4T_2$ absorption band. The chromium fluorescence $^4T_2 \rightarrow {}^4A_2$ decays exponentially in the absence of Tm^{3+} ions, but non-exponentially when Tm^{3+} ions are present. The non-exponential character of the decays increases with the Tm^{3+} concentration and the decays shorten strongly. This is of course related to the $Cr^{3+} \rightarrow Tm^{3+}$ energy transfers.

In order to describe the transfers, we have supposed that each $^4T_2$ Cr^{3+} excited ion was surrounded by a statistically uniform distribution of Tm^{3+} ions in their $^3H_6$ ground state, and that a dipole–dipole type of interaction was responsible for the $Cr^{3+} \rightarrow Tm^{3+}$ energy transfer. This case was first studied by Förster [20] and is usually treated using the well known Inokuti and Hirayama expression [21]:

$$N_1(t) = N_1(0)\exp[-t/\tau_1 - \tfrac{4}{3}\pi^{3/2}CR_0'^3(t/\tau_1)^{1/2}] \tag{17}$$

where N is the $^4T_2$ Cr^{3+} population, C is the Tm^{3+} acceptor concentration given in table 2, τ_1 represents the lifetime of the $^4T_2$ Cr^{3+} donor and R_0' is the radius of the sphere of influence around the Cr^{3+} donor.

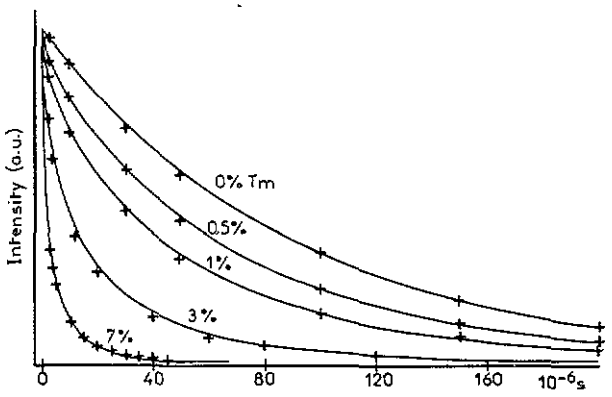

Figure 5. *The $^4T_2 \rightarrow {}^4A_2$ fluoresence decays of Cr^{3+} at room temperature for various Tm^{3+} concentrations. Full curves represent the best fits to experimental data (+).*

The best fit to the five experimental decays (figure 5) has been obtained with the values $\tau_1 = 90 \pm 1\ \mu s$ and $R_0' = 9.4 \pm 0.1$ Å. The quantum yield η_T of the $Cr^{3+} \rightarrow Tm^{3+}$ energy transfer is given in table 3; η_T is close to 1 for $C = 7\%$.

Let us examine now the excited-state dynamics of the $^3H_4$ state of the Tm^{3+} acceptor. This dynamics is complicated by the $Tm^{3+} \rightarrow Tm^{3+}$ cross-relaxation process in which Tm^{3+} ion acts as a donor. This means that each Tm^{3+} ion belongs with probability $W(\varphi)\,d\varphi$ to a class of ions characterized by a de-excitation rate φ due to the cross-relaxation. The normalized function $W(\varphi)$ $(\int_0^\infty W(\varphi)\,d\varphi = 1)$ can be calculated by Markov's procedure (see appendix). In the case of dipole–dipole interaction, this function is given by

$$W(\varphi) = (b/2\pi^{1/2})\varphi^{-3/2} \exp(-b^2/4\varphi) \tag{18}$$

where b is given by equation (4).

In order to simplify the model, we have neglected the energy diffusion among the Tm^{3+} ions but taken into account the cross-relaxation. In this case, the variation rate of the population $N_{2\varphi}(t)$ of the class of Tm^{3+} ions characterized by the cross-relaxation rate φ is

$$\dot{N}_{2\varphi}(t) = -N_{2\varphi}(1/\tau_2 + \varphi) - (N_1/\tau_1 + \dot{N}_1)W(\varphi) \tag{19}$$

where N_1 is given by equation (17). The solution of (19) is then similar to expression (16):

$$N_{2\varphi}(t) = N_1(0)W(\varphi)\exp[-t(1/\tau_2 + \varphi)] - W(\varphi)N_1(t) + \left(\frac{1}{\tau_2} + \varphi - \frac{1}{\tau_1}\right) \times \int_0^t W(\varphi)N_1(t')\exp[-(t-t')(1/\tau_2 + \varphi)]\,dt'. \tag{20}$$

The integration of $N_{2\varphi}(t)$ over φ gives the total population $N_2(t)$ of the $^3H_4$ level. Taking into account (A8), (A9) and (A10), we obtain

$$N_2(t) = N_1(0)\exp[-t/\tau_2)bt^{1/2}] - N_1(t) + \int_0^t N_1(t')\exp\left(-\frac{(t-t')}{\tau_2} - b(t-t')^{1/2}\right) \times \left[\left(\frac{1}{\tau_2} - \frac{1}{\tau_1}\right) + \tfrac{1}{2}b(t-t')^{-1/2}\right] dt'. \tag{21}$$

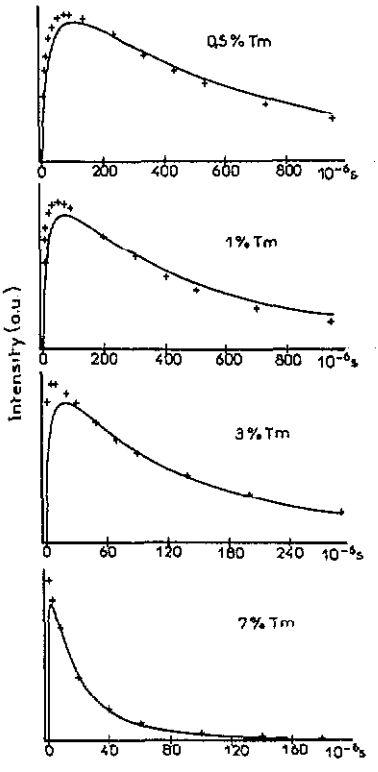

Figure 6. Time dependence of the $^3H_4 \rightarrow {}^3H_6$ fluorescence at room temperature under the $^4T_2$ Cr^{3+} excitation for various Tm^{3+} concentrations.

This equation (21) is used to fit the experimental data illustrated in figure 6. One can see that the dynamics is correctly described only for weak Tm^{3+} concentrations where the $Tm^{3+} \rightarrow Tm^{3+}$ energy diffusion is weak. It is evident that, for Tm^{3+} concentrations greater than 1%, diffusion must be involved but then the solution of the rate equation is not easy.

5. Conclusions and prospects

We have grown (Ca, Zr)-substituted GGG doped with Cr^{3+} and Tm^{3+} ions and analysed the $Tm^{3+} \rightarrow Tm^{3+}$ and $Cr^{3+} \rightarrow Tm^{3+}$ energy transfer mechanisms.

We have also grown the same garnets doped with Cr^{3+}, Tm^{3+} and Ho^{3+} ions, and the study of the energy transfer dynamics is now in progress.

This work is the first step in our search for new holmium-doped gadolinium garnet laser crystals presenting as good as possible match between the $^4T_2$ emission of Cr^{3+} donor and the $^3H_4$ absorption of Tm^{3+} acceptor (which acts as a donor for Ho^{3+} ion). The growth and optical study of holmium-doped (Ca, Mg, Zr)-substituted GGG and other new garnet systems is going on. By comparing the energy transfer efficiencies in all these systems, we should be able to select the best ones for 2 μm laser materials.

Acknowledgment

This work was supported by the Defence Ministry (France), DGA/DRET, under Grant 88/133.

Appendix

The total transfer rate φ of a donor ion is the sum of the transfer rates T_{DA_i} on each acceptor ion A_i of the sample:

$$\varphi = \sum^{N_A} T_{DA_i}(r_i) \tag{A1}$$

where N_A is the total number of acceptor ions and r_i is the distance between D and A_i ions. Because r_i is a random number, φ is also a random number that extends between zero and infinity. The question here is to calculate the probability $W(\varphi)\,d\varphi$ for the transfer rate of a given ion D to have the preassigned value φ, since the probability $\tau(r)$ to find an acceptor ion A at distance r from D is known.

Following Chandrasekhar [22], we shall use Markov's method. It consists of calculating first the Fourier transform $A_{N_A}(\rho)$ of $W(\varphi)$ with the formula

$$A_{N_A}(\rho) = \left(\int_0^R \exp[i\rho T_{DA}(r)]\tau(r)\,dr\right)^{N_A} \tag{A2}$$

where R is the radius of the sample supposed to be a sphere.

Assuming a uniform random distribution for the acceptor ions A_i around the donor ion D, $\tau(r) = 3r^2/R^3$, we shall let R and N_A tend to infinity simultaneously in such a way that the concentration C_A of acceptor ions A_i is constant: $C_A = \frac{4}{3}\pi R^3/N_A$. In this case (A2) becomes

$$A(\rho) = \exp\left(-4\pi C_A \int_0^\infty \{1 - \exp[i\rho T_{DA}(r)]\} r^2\,dr\right). \tag{A3}$$

We now consider the case of a multipolar interaction between D and A: $T_{DA}(r) = C_{DA}/r^s$ ($s = 6$, 8, 10 for dipole–dipole, dipole–quadrupole, quadrupole–quadrupole interaction). By using Cauchy's residue theorem the result will be

$$A(\rho) = \exp[-b(-i\rho)^{3/5}] \tag{A4}$$

with

$$b = \tfrac{4}{3}\pi C_A C_{DA}^{3/5}\Gamma(1 - \tfrac{3}{5})$$

where Γ is the Euler function defined by

$$\Gamma(t) = \int_0^\infty e^{-x}x^{t-1}\,dx.$$

The probability $W(\varphi)$ is then given by the Fourier transform of $A(\rho)$ as

$$W(\varphi) = \frac{1}{2\pi}\int_{-\infty}^{\infty} \exp[-i\rho\varphi - b(-i\rho)^{3/5}]\,d\rho. \tag{A5}$$

In the case of interest here $s = 6$ and if we change the variable of integration to $x = \rho^{1/2}$ and use Cauchy's theorem we find

$$\begin{aligned} &W(\varphi) = (b/2\pi^{1/2})\varphi^{-3/2}\exp(-b^2/4\varphi) && \text{if } \varphi \geq 0 \\ &W = 0 && \text{if } \varphi < 0. \end{aligned} \tag{A6}$$

The time evolution of the donor ion population $N_D(t)$ is the superposition of the exponential evolutions of each class of donor ions characterized by transfer rate φ:

$$N_D(t) = N_D^0 \int_0^\infty W(\varphi)\exp[-t(1/\tau_D + \varphi)]\,d\varphi. \tag{A7}$$

Expression (A5) leads to the following properties of $W(\varphi)$:

$$\int_0^\infty W(\varphi)\,\mathrm{d}\varphi = 1 \tag{A8}$$

$$\int_0^\infty W(\varphi)\,\mathrm{e}^{-t\varphi}\,\mathrm{d}\varphi = \mathrm{e}^{-bt^{1/2}} \tag{A9}$$

$$\int_0^\infty \varphi W(\varphi)\,\mathrm{e}^{-t\varphi}\,\mathrm{d}\varphi = \tfrac{1}{2}bt^{-1/2}\,\mathrm{e}^{-bt^{1/2}}. \tag{A10}$$

By taking account of (A9), expression (A7) leads to the well known Hinokuti and Hirayama formula (17).

References

[1] Chicklis E P, Naiman C S, Folweiler R C and Doherty J C 1972 *IEEE J. Quantum Electron.* **QE-8** 225
[2] Knights M G, Mosto J and Chicklis E P 1985 *Conf. on Lasers and Electro-Optics (1985 Tech. Digest Ser.)* (Washington, DC: Optical Society of America) p 94
[3] Antipenko B M, Glebov A S, Kiseleva T I and Pis'mennyi V A 1985 *Sov. Tech. Phys. Lett.* **11** 284
[4] Allat'ev A N, Zharikov E V, Kalitin S P, Laptev V V, Osiko V V, Ostroumov V G, Prokhorov A M, Saidov Z S, Smirnov V A, Sorokina I T, Umyskov A F and Shcherbakov I A 1986 *Sov. J. Quantum Electron.* **16** 1404
[5] Duczynski E W, Huber G, Ostroumov V G and Shcherbakov I A 1986 *Appl. Phys. Lett.* **48** 1562
[6] Allen R, Esterowitz L, Goldberg L and Weller J F 1986 *Topical Meeting on Tunable Solid State Lasers 86: 9* (Washington, DC: Optical Society of America) p 144
[7] Kintz G J 1989 *Conf. on Lasers and Electro-Optics (1989 Tech. Digest Ser.)* vol 11 (Washington, DC: Optical Society of America) p 54
[8] Becker T, Clausen R, Huber G, Duczynski E W and Mitzecherlich P 1989 *Tunable Solid State Lasers (Tech. Digest)* (Washington, DC: Optical Society of America) pp 183–5
[9] Stoneman R C and Esterowitz L 1989 *Conf. on Lasers and Electro-Optics (1989 Tech. Digest Ser.)* vol 11 (Washington, DC: Optical Society of America) p 54
[10] Mateika D, Herrnring J, Rath R and Rusche Ch 1975 *J. Cryst. Growth* **30** 311
[11] Allibert M, Chatillon C, Mareschal J and Lissalde F 1974 *J. Cryst. Growth* **23** 289
[12] Brandle C D, Miller DC and Nielsen J W 1972 *J. Cryst. Growth* **12** 195
[13] Brandle C D, Fratello V J and Valentino A J 1987 *J. Cryst. Growth* **85** 223
[14] Boulon G, Garapon C and Monteil A 1987 *Advances in Laser Science–II (AIP Conf. Proc. 160)* (New York: American Institute of Physics) p 104
[15] Antipenko B M 1984 *J. Tech. Phys.* **54** 385
[16] Brenier A, Rubin J, Moncorge R and Pedrini C 1989 *J. Physique* **50** 1463
[17] Grant J C W 1971 *Phys. Rev.* B **4** 648
[18] Yokota M and Tanimoto O 1967 *J. Phys. Soc. Japan* **22** 779
[19] Bloembergen N 1949 *Physica (Utr.)* **15** 386
[20] Förster Th 1949 *Z. Naturf.* a **4** 321
[21] Inokuti M and Hirayama F 1965 *J. Chem. Phys.* **43** 1978
[22] Chandrasekhar S 1943 *Rev. Mod. Phys.* **15** 1